

Anthraquinone Flow Battery Reactants with Nonhydrolyzable Water-Solubilizing Chains Introduced via a Generic Cross-Coupling Method

Yan Jing, Eric M. Fell, Min Wu, Shijian Jin, Yunlong Ji, Daniel A. Pollack, Zhijiang Tang, Dian Ding, Meisam Bahari, Marc-Antoni Goulet, Tatsuhiro Tsukamoto, Roy G. Gordon,* and Michael J. Aziz*



Cite This: *ACS Energy Lett.* 2022, 7, 226–235



Read Online

ACCESS |



Metrics & More

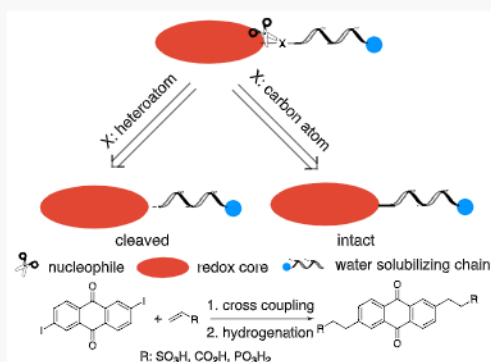


Article Recommendations



Supporting Information

ABSTRACT: Water-soluble anthraquinones (AQs) hold great promise serving as redox-active species in aqueous organic flow batteries. Systematic investigations into how the properties of redox molecules depend on the water-solubilizing groups (WSGs) and the way in which they are bound to the redox core are, however, still lacking. We introduce WSGs linked to anthraquinone by C=C bonds via a cross-coupling reaction and convert C=C to C–C bonds through hydrogenation. The anthraquinone and the WSGs are connected via (un)branched chains with (un)saturated bonds. We investigate the influence of chains and ionic ending groups on the redox potentials of the molecules and identify three important trends: (1) The electron-withdrawing ending groups can affect the redox potentials of AQs with two unsaturated hydrocarbons on the chains through π -conjugation. (2) For chains with two (un)saturated straight hydrocarbons, WSGs increase the redox potentials of the AQs in the order $\text{PO}_3^{2-} < \text{CO}_2^- < \text{SO}_3^-$. (3) AQs with (un)saturated chains at high pH possess desirably low redox potentials, high solubilities, and high stability. Disproportionation leads to the formation of anthrone, which can be regenerated to anthraquinone. Tautomerization results in the saturation of alkene chains, stabilizing the structure. We utilize these observations to identify a potentially low-cost and long-lifetime negative electrolyte that demonstrates a temporal fade rate as low as 0.0128%/day when paired with a potassium ferrocyanide positive electrolyte.



Energy storage systems have become an integral part of modern society.^{1,2} Among the most promising electricity storage systems are aqueous redox flow batteries (ARFBs). Featuring intrinsically nonflammable electrolytes and decoupled energy and power scaling, ARFBs can play a crucial role in storing massive amounts of electricity produced from intermittent renewable resources such as solar energy and wind power and releasing the electricity when it is needed. Among a variety of ARFBs, the vanadium redox flow battery (VRFB) has been the most developed and mature system to date.^{3,4} Redox-active organic molecules composed of earth-abundant elements such as carbon, hydrogen, oxygen, nitrogen, and sulfur are potentially cost-effective.^{5,6} Furthermore, because of the structural diversity and tunability of organic molecules, molecular engineering can be employed to judiciously design desired redox molecules for aqueous organic redox flow batteries (AORFBs).^{7,8} Although extremely stable anthraquinone-based aqueous flow batteries have been developed with projected decadal lifetime,⁹ manufacturing costs remain challenging.

Additionally, the technology still stands to benefit greatly from improved synthetic methods, as well as systematic investigations into how the properties of redox molecules depend on the water-solubilizing groups and the way in which they are bound to redox cores.

Water-soluble quinone derivatives used for AORFBs comprise two motifs, the hydrophobic quinone redox center and the hydrophilic water-solubilizing groups, including $-\text{SO}_3^-$,⁶ $-\text{CO}_2^-$,¹⁰ $-\text{PO}_3^{2-}$,¹¹ $-\text{NR}_4^+$,^{12,13} $-\text{O}^-$,⁷ and polyethylene glycol (PEG).¹⁴ These motifs are connected via covalent bonds such as C–O,¹⁴ C–S,¹⁵ and C–C⁹ or are directly attached to redox

Received: November 17, 2021

Accepted: December 8, 2021

Scheme 1. (a) Retrosynthetic Analysis of $-C_2H_4-$ Linked Water-Soluble Anthraquinones (AQs). (b) Synthetic Routes and Conditions Used for the Synthesis of a Class of Water-Soluble AQs. (c) Water-Soluble AQs Synthesized by the Same Method

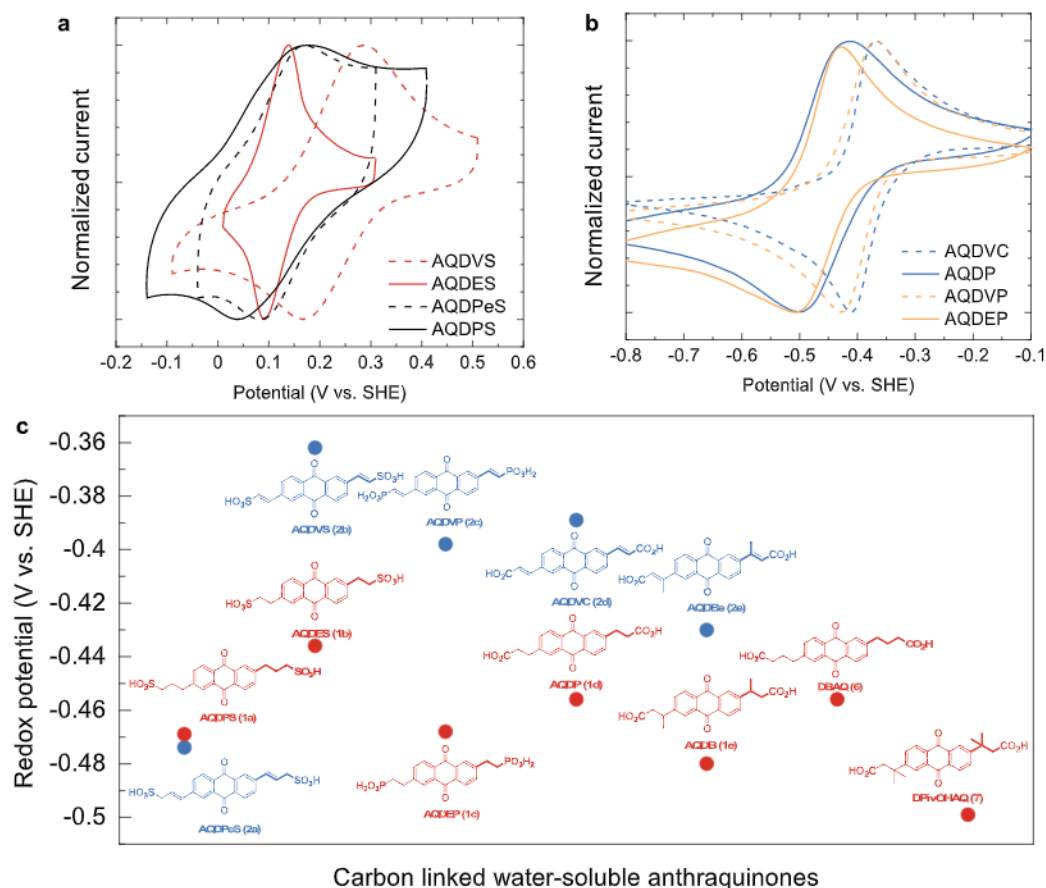
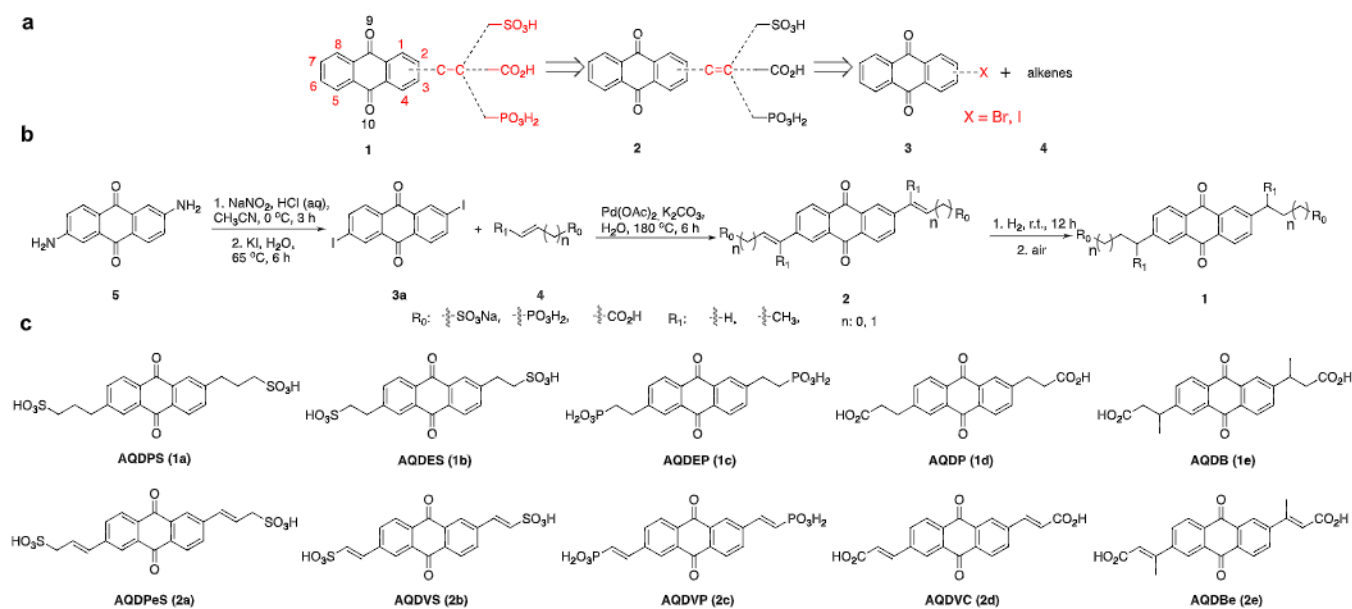


Figure 1. Cyclic voltammograms (CVs) on glassy carbon and redox potentials of the water-soluble AQs: (a) CVs of AQDVS, AQDES, AQDPeS, and AQDPS in 1 M H_2SO_4 ; (b) CVs of AQDVC, AQDP, AQDVP, and AQDEP in 1 M KOH. Scan rate: 100 mV/s. Concentration of AQs: 5 mM. (c) Mapping the redox potentials of 12 water-soluble anthraquinones at pH 14, including two previously reported carbon-linked AQs: DPivOHAQ, 3,3'-(9,10-anthraquinone-diyl)bis(3-methylbutanoic acid); DBAQ, 4,4'-(9,10-anthraquinone-diyl)dibutanoic acid.^{9,22} The AQs with saturated chains are red, and the AQs with unsaturated chains are blue. All CV measurements were collected at room temperature with a scan rate of 100 mV/s.

cores.^{6,7,16,17} It appears that redox cores bonded to water-solubilizing groups via C–heteroatom bonds are susceptible to

nucleophilic substitution reactions, resulting in the detachment of water-solubilizing groups from redox cores.^{10,18,19} Because

Table 1. Properties of Carbon-Linked Water-Soluble AQs^a

Molecule	Number	Chains	Redox potential @ pH 14 (V)	Peak separation (mV)	Solubility (M)
AQDPS	1a		-0.469	50	0.30 @ pH 7
AQDPeS	2a		-0.474	138	0.35 @ pH 7
AQDES	1b		-0.436	53	1.10 @ pH 0 0.30 @ pH 7
AQDVS	2b		-0.362	63	0.10 @ pH 0
AQDEP	1c		-0.468	80	1.10 @ pH 12
AQDVP	2c		-0.398	56	0.85 @ pH 12
AQDP	1d		-0.456	83	1.00 @ pH 12
AQDVC	2d		-0.389	42	0.70 @ pH 12
AQDB	1e		-0.480	98	0.77 @ pH 12
AQDBe	2e		-0.430	86	0.65 @ pH 12
DBAQ	6		-0.456	83	1.00 @ pH 12
DPIvOHAQ	7		-0.499	52	0.75 @ pH 12

^aThe pH was adjusted by KOH or H₂SO₄.

carbon-carbon bonds are more chemically resistant against nucleophilic attack than carbon-heteroatom bonds such as C-O (S, N), it is desirable to incorporate carbon-carbon bonds between redox centers and water-solubilizing ending groups.⁹ Redox centers and -SO₃⁻, -CO₂⁻, and -PO₃²⁻ water-solubilizing groups are considered electron-withdrawing because of their resonance and negative inductive effects. When there is only a single unsubstituted methylene group (-CH₂-) between a redox center and a water-solubilizing group, the close proximity of the electron-withdrawing groups to the redox core may cause molecules to be vulnerable to nucleophilic attack.^{13,20,21} In contrast, excellent molecular stability has been achieved when there are at least two carbon atoms between water-solubilizing groups and redox cores.^{9,13}

Here we demonstrate a generic method for synthesizing water-soluble anthraquinone (AQ) derivatives with saturated or unsaturated and branched or straight carbon linkages (Scheme 1). Specifically, 2,6-diamino-9,10-anthraquinone is transformed to 2,6-diiodo-9,10-anthraquinone. Then, C=C linked water-solubilizing groups are introduced via Heck cross-coupling reactions to afford water-soluble anthraquinones with unsaturated carbon linkages. Hydrogenation of these molecules then converts C=C bonds to C-C bonds. Using the same synthetic method, we synthesized ten anthraquinone derivatives, each with one of three water-soluble ending groups (-SO₃⁻, -CO₂⁻, or -PO₃²⁻) and a particular (branched/straight, unsaturated/saturated) carbon linkage. We evaluated their solubility, stability, redox potentials, standard rate constants, and diffusion coefficients to better understand the effects of different solubilizing groups and linkages. In the end, we identified 9,10-anthraquinone-2,6-dipropionic acid (AQDP) as an extremely stable and potentially low-cost negative electrolyte (negolyte). When paired with potassium ferrocyanide positive electrolyte (posolyte), AQDP exhibits a temporal fade rate as low as 0.012% per day.

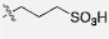
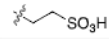
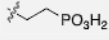
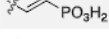
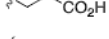
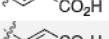

Following the reasoning that a stable redox molecule should have at least two carbons between a redox core and a water-solubilizing group, we consider Heck cross-coupling to be a plausible route to access the desired water-soluble anthraqui-

ones (1 and 2). Specifically, halogenated anthraquinones (3) can react with easily accessible water-soluble alkenes (4) to afford anthraquinones bearing water-solubilizing groups separated from the anthraquinone core by at least two carbons, and the tethered alkenyl chains can be saturated via hydrogenation (Scheme 1). We selected a variety of alkenes (4) containing SO₃⁻, CO₂⁻, and PO₃²⁻ ending groups to react with 3. First, 2,6-diaminoanthraquinone (5) is converted to 2,6-diiodoanthraquinone (3a) through the intermediate diazotization (Scheme 1b). Then 3a was subjected to palladium-catalyzed Heck cross-coupling reactions using different water-solubilizing coupling partners to afford 2a-2e. After completion of the Heck reaction, without further purification, hydrogen gas was introduced in the reaction to afford 1a-1e through a one-pot hydrogenation-ambient autoxidation sequence to convert alkene bonds to alkanes and subsequently oxidize anthrahydroquinones to anthraquinones. Scheme 1c lists all carbon-linked AQs synthesized by this method. Both unsaturated and saturated as well as branched and straight hydrocarbon chains were introduced; the number of carbon atoms on each chain is 2-4.

Figure 1 shows the cyclic voltammogram (CV) results of AQs at pH 0 and 14 and a map of redox potentials at pH 14. For those AQs with two unsaturated hydrocarbons on the chains, the electron-withdrawing ending groups (SO₃⁻, PO₃²⁻, and CO₂⁻) can still affect the redox potentials through π -conjugation. Consequently, the redox potentials of AQDVS (2b), AQDVP (2c), and AQDVC (2d) are 60-80 mV higher than those of the saturated AQs, i.e., AQDES (1b), AQDEP (1c), and AQDP (1d), where the negative resonance effect is weakened due to the saturated hydrocarbon linkage. We also noticed that those molecules show a clear trend in redox potentials, i.e., 2b > 2d > 2c for the unsaturated AQs and 1b > 1d > 1c for the saturated AQs (Figure 1c), which is supported by the theoretical calculation of water-solubilizing groups increasing redox potentials in the order SO₃⁻ > CO₂⁻ > PO₃²⁻.²³

Interestingly, AQDPeS (2a) has a slightly lower redox potential than its saturated analogue AQDPS (1a). This effect may be explained by the two unsaturated C=C bonds extending the conjugation of the anthraquinone core and enhancing the

Table 2. Properties of Carbon-Linked Water-Soluble AQs (cont.)^a

Molecule	Number	Chains	Diffusion coefficient (cm ² /s)		k_o (cm/s)		α from RDE
			from CV (underestimate)	from RDE	from CV (simulate)	from RDE	
AQDPS	1a		5.6e-7	9.8e-7	4.5e-3	3.0e-3	0.74
AQDES	1b		4.3e-8	1.3e-7	1.5e-3	4.0e-3	0.50
AQDEP	1c		2.5e-7	8.6e-7	1.5e-3	1.4e-3	0.72
AQDVP	2c		6.5e-7	1.1e-6	6.5e-3	2.2e-3	0.65
AQDP	1d		1.8e-7	9.5e-7	1.6e-3	3.4e-3	0.72
AQDVC	2d		6.2e-7	1.1e-6	5.3e-3	3.3e-3	0.61
AQDBe	2e		2.8e-8	3.8e-7	1.9e-3	5.5e-3	0.66

^aAll molecules were prepared with a concentration of 5 mM and tested at pH 14.

resonance effect in **2a**; meanwhile, the saturated methylene group may weaken the negative resonance effect of SO_3^- . The same trend is also found at pH 0; the potential of **1b** (110 mV vs SHE) is 115 mV lower than that of **2b** (225 mV vs SHE), whereas the potential of **1a** (122 mV vs SHE) is slightly higher than that of **2a** (98 mV vs SHE) (Figure 1a).

The effect of branched alkyl chains on the redox potentials can be evaluated through the comparison of **1d**, AQDB (**1e**), and DPivOHAQ (**7**).⁹ Addition of electron-donating methyl groups on the benzylic carbons can lead to lower redox potentials of AQs, with the order of potentials given by **7** (−0.499 V) < **1e** (−0.480 V) < **1d** (−0.456 V). A similar trend is also found from the unsaturated AQs, i.e., AQDBe (**2e**) (−0.430 V) < **2d** (−0.389 V).

For those AQs possessing saturated and straight chains with different numbers of carbon atoms, the redox potential of **1a** (−0.469 V) is 33 mV lower than that of **1b** (−0.436 V), whereas the redox potential of **1d** (−0.456 V) is the same as that of DBAQ (**6**) (−0.456 V) at pH 14 (Figure 1c). The difference suggests that the inductive electron-withdrawing effect of CO_2^- can be sufficiently weakened by two saturated carbons, whereas SO_3^- still plays a role in elevating the redox potential even when distanced by two saturated carbons. The kinetic contributions to the difference in the measured redox potentials between **1a** and **1b** at pH 14 should be small, as the peak separations in both the cyclic voltammograms (CVs) of **1a** and **1b** in Figures S16c and S19c are less than 50 mV, suggesting that both compounds have fast electrochemical reaction kinetics in base, whereas the Koutecký-Levich analysis (Figure S17) implies that there might be an overpotential associated with at least one of the measured potentials.

The redox potentials of **1a** and **1b** are similar in acid (Figure 1a), indicating that the influence of SO_3^- on the redox potential of AQ at pH 0 is sufficiently isolated by the saturated carbons, whereas the CV peak separations of **1b** and **1a** are ~50 mV and ~120 mV, respectively, suggesting that the two compounds have different electrochemical reaction kinetics in acid. Given that anthraquinones undergo proton-decoupled two-electron transfer in strong base but proton-coupled two-electron transfer in strong acid and that **1a** has one more methylene group on each chain than does **1b**, the difference in peak separation in acid could be associated with overpotentials incurred due to different mass transfer coefficients.

The aqueous solubility of AQs depends on solution pH, ending groups, and the chains with (un)saturated, (un)branched hydrocarbons between the redox cores and the ending groups. The solubilities of these AQs are summarized in Table 1. The solubility of **1b** reaches 1.10 M at pH 0 due to the negative pK_a of $-\text{SO}_3\text{H}$, whereas its solubility decreases to 0.30 M when the pH is adjusted to 7 by adding KOH. Similarly, the solubility of anthraquinone-2,7-disulfonic acid (AQDS) is 1.50 M at pH 0,⁶ and its solubility decreases to 0.58 M at pH 7 when the pH is adjusted by adding NaOH.²⁴ At pH 12, $-\text{CO}_2\text{H}$ and $-\text{PO}_3\text{H}_2$ are fully deprotonated, and the solubilities of **1c**, **1d**, and **6** at pH 12 reach 1.1 M, 1.0 M, and 1.0 M, respectively. AQs with unsaturated chains usually show lower solubilities than their saturated versions, i.e., **1b** > **2b**, **1c** > **2c**, **1d** > **2d**. A plausible explanation is that the extended conjugation in the unsaturated AQs enhances the intermolecular π – π interactions, thus lowering their solubility in water. In addition, the solubility of AQs tends to decrease when more hydrophobic hydrocarbons are incorporated to chains. For example, the solubility of **2e** is lower than that of **2c** as one extra branched methyl group is introduced in **2e**. Similarly, the solubility of **6** is slightly lower than that of **1d** as there are three methylene groups between the AQ and the ending groups in **6** and two in **1d**.

The electrochemical kinetics of seven AQs were investigated; in particular, their rate constants and diffusion coefficients were extracted from cyclic voltammetry and rotating disc electrode experiments (Figures S16–30, Supporting Information). CVs were evaluated at multiple scan rates in pH 14 supporting electrolyte, with all molecules investigated demonstrating quasi-reversible, two-electron redox processes. Using the Randles–Ševčík equation, a plot of voltammogram peak currents versus the square root of scan rate provides a slope from which a diffusion coefficient can be calculated. However, it must be noted that by using the Randles–Ševčík equation, the diffusion coefficient will be underestimated whenever the observed redox process is not fully reversible, as is always the case in this study. Therefore, linear sweep voltammetry with a rotating disk electrode was used to determine more accurate values for the diffusion coefficients. Using these diffusion coefficients, CVs were then fit by simulation²⁵ to the experimental data to determine the electrochemical rate constants of the limiting reduction process (k_o) and the formal reduction potentials of the individual electron redox processes (E^0_1 , E^0_2). The rate

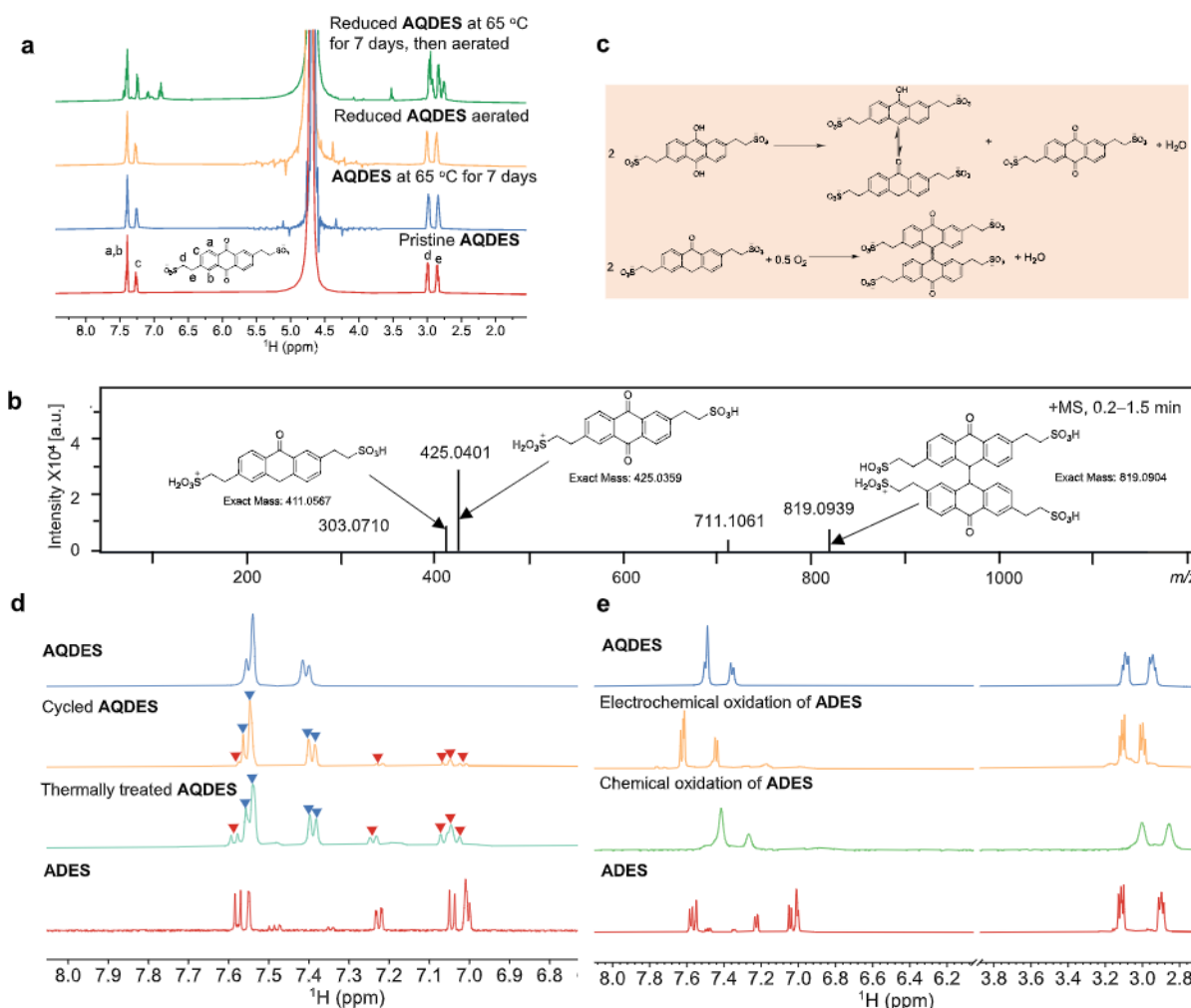


Figure 2. Structural stability studies of 1b and its reduction product in 1 M H₂SO₄. (a) Thermal stability as evaluated by ¹H NMR spectroscopy. 1b is thermally stable at elevated temperatures (65 °C) over 7 days, whereas the reduction product of 1b is thermally unstable, as indicated by the decomposition peaks. The signal at 4.79 ppm is from the solvent (water). (b) Mass spectrum suggesting the formation of anthrone and anthrone dimer derivatives. Positively ionized (protonated), m/z = exact mass of protonated molecules with one positive charge. (c) Proposed decomposition pathways in which the decomposition compounds were detected by mass spectrometry. (d) Stacked ¹H NMR of (from top to bottom) pristine, cycled, thermally treated (reduction product treated at 65 °C for 7 days, then aerated) AQDES and chemically synthesized diethylsulfonated-2,6-anthrone (anthranol) (ADES), suggesting that the decomposition compound in the cycled and thermally treated AQDES is ADES. (e) Stacked ¹H NMR of (from top to bottom) pristine AQDES, electrochemically oxidized AQDES from ADES, chemically oxidized AQDES from ADES by CrO₃ in acidic conditions, and ADES, suggesting that ADES can be (electro)chemically oxidized to AQDES.

constants determined from CV simulation and RDE were both in good agreement with each other (see Table 2). As others have noted, *ex situ* electrochemical characterization of ARFB active species is almost always performed on flat macroelectrodes (e.g., glassy carbon), yet these molecules are then tested in flow batteries with porous carbon electrodes of varied surface composition where electron transfer kinetics quantification is further complicated by mass transport.^{26–28} Thus, the electrochemical kinetics of these AQs may differ when porous carbon electrodes are used in a flow battery, possibly even resulting in slower electrochemical kinetics.^{29,30}

The structure–property relationships between AQs and their redox potentials and solubilities have been evaluated in detail; all the tested AQs show similar standard rate constants and diffusion coefficients. Plausible explanations for the similar rate constants are AQ cores dominate and the chains are not bulky enough to provide steric hindrance; the linking manners and water-solubilizing groups appear not to affect the rate constants; the extension of the π system in the unsaturated AQs over the

saturated ones does not affect the rate constants of AQs. Additionally, it is unlikely that a significant difference in the standard rate constants would be observed given that minimal solvation reorganization upon reduction/oxidation, typical for AQs, allows for fast electrochemical kinetics.³¹

All AQs show similar diffusion coefficients because all the AQ molecules have very similar molecular sizes.

Chief among the degradation mechanisms that limit the lifetime of organic flow batteries is the molecular decomposition of the organic species themselves. In addition to cost and resource limitations, technical challenges restrict the length of cycling experiments at the lab scale to assess the intrinsic stability of these reactants. Accelerating these decomposition mechanisms through higher temperature experiments is the most direct way to accelerate research and development of new viable compounds.^{32,33}

The stability of redox molecules is of utmost importance because it determines whether the molecule is eventually useful for real applications. It is thus necessary to independently

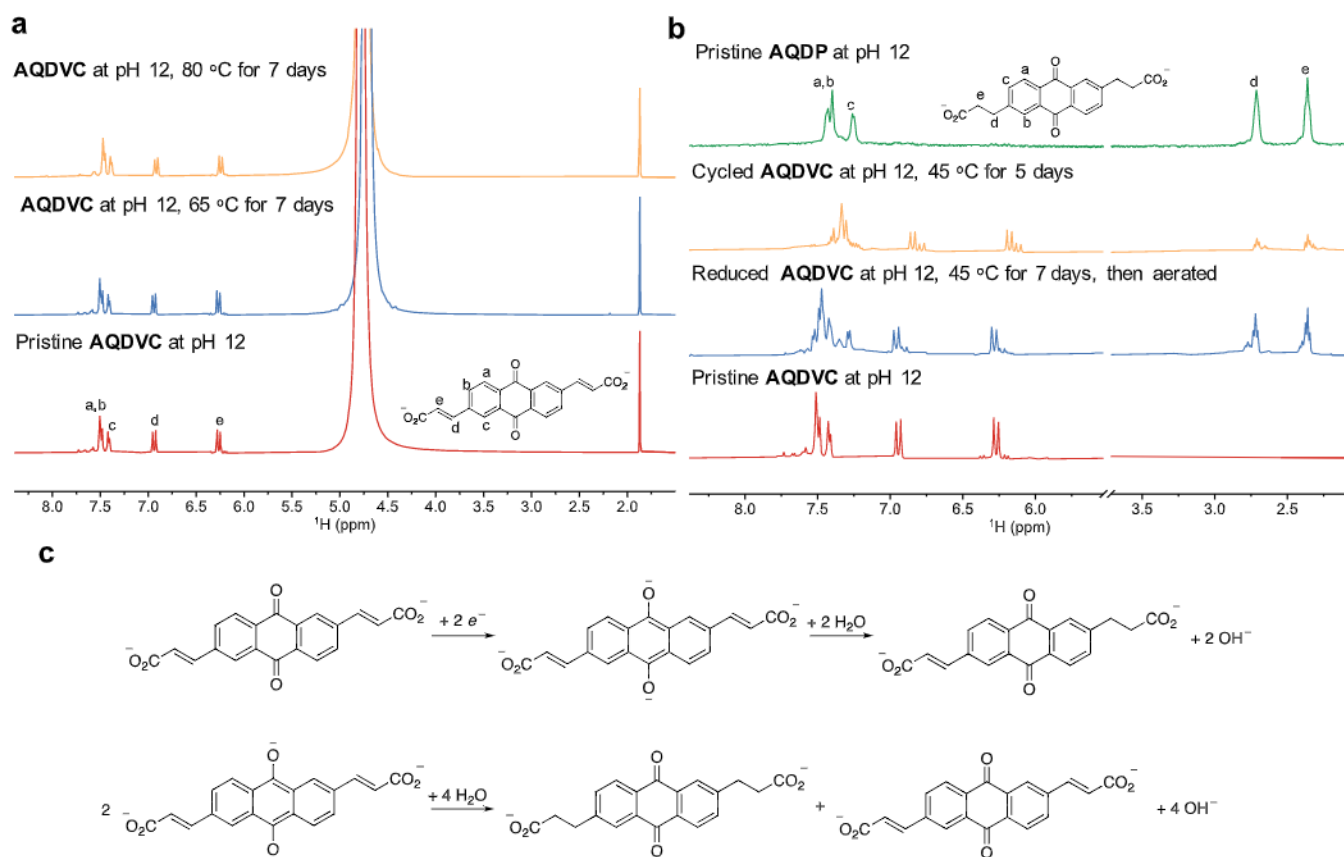


Figure 3. Structural stability studies of **2d** and its reduction product at pH 12. Thermal stability was measured by ^1H NMR spectroscopy. (a) **2d** at pH 12 is thermally stable at elevated temperatures (65 °C) over 7 days. The signal at 1.85 ppm is from the internal standard (potassium acetate), and the signal at 4.79 ppm is from the solvent (water). (b) The reduction product of **2d** at pH 12 is thermally unstable at 45 °C after 7 days and unstable when cycled at 45 °C for 5 days, as indicated by the appearance of new peaks in both the aromatic and aliphatic regions. The chemical shifts of the new peaks are either similar or identical to those of **1d**, suggesting that the reduction product of **2d** may tautomerize to molecules similar to **1d**. (c) Decomposition compounds were detected by LC-MS, and proposed possible decomposition pathways are illustrated (see the [Supporting Information](#)).

evaluate the stability of a redox molecule before running a full cell in which counter electrolytes, the membrane, and electrodes will be involved and complicate the analysis. A protocol that has proven to be effective is to store electrolytes with different states of charge (SOC) at reasonably elevated temperatures and operational pH, which can accelerate the molecular decompositions of both states. Depending on the decomposition rates, decomposition compounds can be detected by liquid chromatography–mass spectroscopy (LC-MS) or ^1H NMR spectroscopy.^{9–11,34}

Given that the redox potential of **1b** is 110 mV vs RHE at pH 0 and the solubility of **1b** is 1.1 M, it is worthwhile to investigate its thermal stability in acid for both redox states. The ^1H NMR spectra in [Figure 2a](#) suggest that **1b** is thermally stable, whereas the reduction product of **1b** is not. The sample showing ^1H NMR decomposition peaks in [Figure 2a](#) was further analyzed by mass spectrometry. The characteristic m/z values ([Figure 2c](#)) suggest decomposition of the reduction product of **1b**; its anthrone and anthrone dimer derivatives ([Figure 2b](#)) were produced over 7 days at 65 °C. These decomposition compounds have been observed in previous studies supported by theoretical calculations.³⁵ To further confirm the formation of anthrone derivatives, we chemically synthesized diethylsulfonated-2,6-anthrone (anthranol) (ADES)³⁵ and found that its ^1H NMR chemical shifts and peak splitting are indeed in line with those in the cycled and thermally treated AQDES spectra

([Figure 2d](#)). We previously found that anthrone derivatives can be chemically oxidized to AQs when exposed to air or other oxidants^{9,35,36} and electrochemically oxidized back to AQs when proper potentials are applied.³⁶ We built an electrochemical cell of 5 mL of 0.05 M ADES paired with 15 mL of 0.1 M AQDS (anthraquinone-2,7-disulfonate) in 1 M H_2SO_4 for ADES electrochemical oxidation. A constant current of 2 mA/cm² was applied until the potential of ADES vs AQDS reached 1.7 V. After that, an aliquot of ADES solution was taken and diluted with D_2O for ^1H NMR measurement. Our preliminary (electro)chemical oxidation results confirmed the conversion of ADES to AQDES ([Figure 2e](#)), suggesting that it would be plausible to *in situ* electrochemically regenerate redox-active AQDES from redox-inactive ADES in flow batteries.

To achieve commercial viability, AORFB electrolytes must be extremely stable and also have a lower capital cost than existing vanadium flow battery electrolytes. Among the AQs reported in the present work, **1d** and **2d** are synthesized from anthraquinone precursor and acrylic acid, with the latter being a major building block in the production of many industrial products. The evaluation of the stability of **2d** in both oxidation states at pH 12 is presented in [Figure 3](#). Although the unchanged spectra in [Figure 3a](#) indicate that **2d** is stable at both 65 °C and 80 °C after 7 days, the new peaks appearing in both the aromatic and aliphatic regions in [Figure 3b](#) suggest that the reduction product of **2d** is unstable when stored at 45 °C for 7 days and when

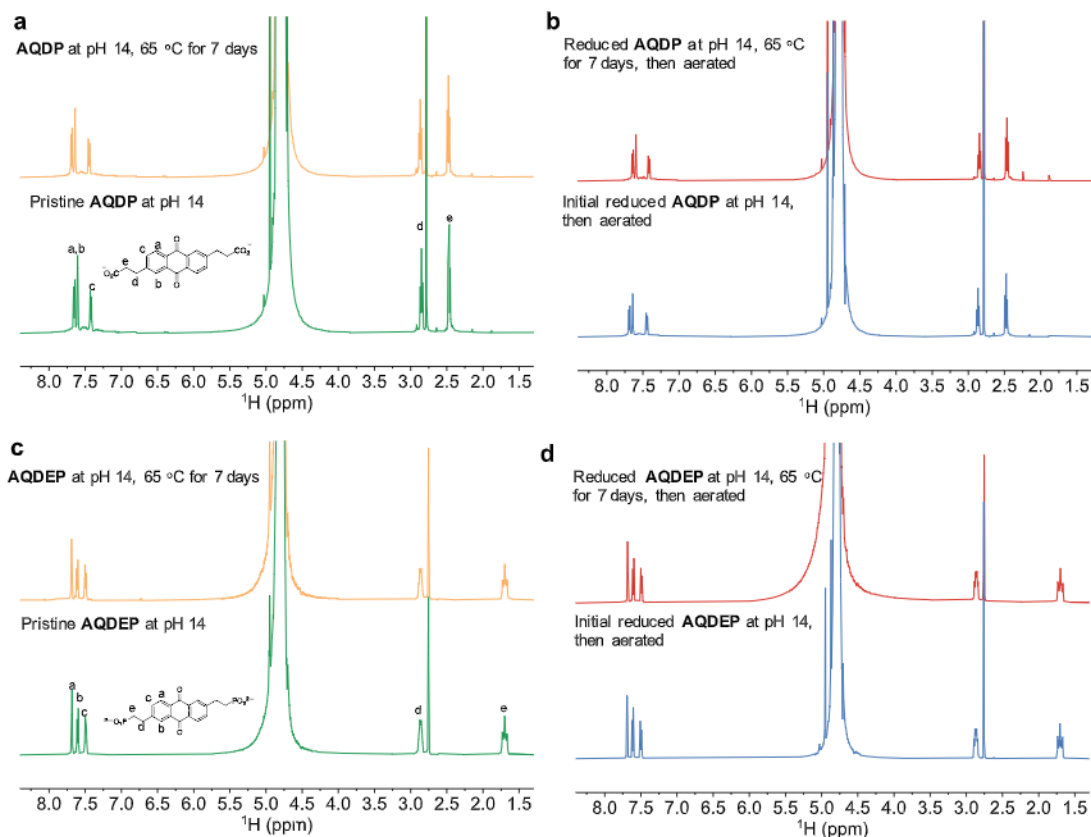


Figure 4. Structural stability studies of the redox pairs **1c** and **1d** at pH 14. Thermal stability at elevated temperature (65 °C) over 7 days was confirmed by ^1H NMR spectroscopy. (a) Stacked ^1H NMR spectra of **1d** at pH 14. (b) Stacked ^1H NMR spectra of the reduction product of **1d** at pH 14 after aeration. (c) Stacked ^1H NMR spectra of **1c** at pH 14. (d) Stacked ^1H NMR spectra of the reduction product of **1c** at pH 14 after aeration. The signal at 2.75 ppm is from the internal standard (sodium methanesulfonate). The signal at 4.79 ppm is from the solvent (water). AQDP, AQDEP, and sodium methanesulfonate were prepared with a concentration of 0.1 M. Unchanged peak integrals of AQDP and AQDEP before and after the thermal treatment relative to the internal standard quantitatively indicate that there is no molecular decomposition at pH 14 at 65 °C over 7 days.

cycled at 45 °C for 5 days (Figure S13). Interestingly, the chemical shifts of the new peaks are either similar or identical to those of **1d**. The m/z ratio obtained from LC-MS experiments suggested the existence of **1d**, **2d**, and a compound with a molecular weight equal to 2 less than that of **1d** (or 2 more than that of **2d**), which we hypothesize is an intermediate possessing one saturated chain and one unsaturated chain. Corresponding reaction mechanisms are proposed in Figure 3c. Tautomerization favors formation of the intermediate, and disproportionation leads to the formation of **1d** and **2d**.^{16,37}

Given the instability of **2d**, we set out to evaluate the stability of the saturated analogues. **1c** and **1d** are two molecules with two saturated hydrocarbon chains. Both the redox states of each were stored at pH 14 and at 65 °C for 7 days and then characterized by ^1H NMR (Figure 4). Identical spectra for the two molecules in both states indicate their excellent thermal stability. By comparing the redox potentials, solubility, rate constants, diffusion coefficients, and stability of all carbon-linked AQs, we notice that at high pH, water-soluble AQs with saturated chains demonstrate lower redox potentials, higher solubility, and better stability than their unsaturated versions; therefore, water-soluble AQs with saturated chains are desirable negolyte active species.

AQDP (**1d**) was chosen to be investigated in full cells given its potential low-cost in mass production, excellent stability, high solubility, and suitable redox potential. The voltage profile and

the cell cycling in Figure 5a and b are from a 0.1 M AQDP full cell when paired with a potassium ferrocyanide polysolite. The full cell approached 94.5% of the theoretical capacity and exhibited a temporal fade rate of 0.0128% per day after being cycled for 8 days and 350 cycles, suggesting that AQDP is extremely stable.³³ The dip highlighted in Figure 5b was caused by the temporary depletion of nitrogen, as the cell was cycled in a nitrogen-filled glovebag. A full cell with 1 M AQDP was built to demonstrate the feasibility of a concentrated flow cell operation. The concentrated cell exhibited a capacity utilization of 79.2% (Figure 5c) and a temporal fade rate of 0.025% per day over 11 days. The lower capacity utilization and the fluctuations in capacity and Coulombic efficiency in Figure 5d are possibly due to the concentration approaching the solubility limit and/or high mass transport resistance.^{10,38} The fade rate of the concentrated cell (1 M AQDP) is approximately twice as high as that of the dilute cell (0.1 M AQDP), and further experimental investigation is required to examine whether the difference in fade rate is due to the difference in concentration.

Polarization curves at various SOC are shown in Figure 5e. AQDP delivers a peak power density exceeding 180 mW/cm² at 90% SOC. The open circuit voltage of the full cell increases with increasing SOC and is approximately 0.98 V at 50% SOC. The high-frequency resistance remains approximately 1.2 Ω cm² over the full SOC range (Figure 5f), which is mainly due to the membrane resistance. The polarization resistance varies from

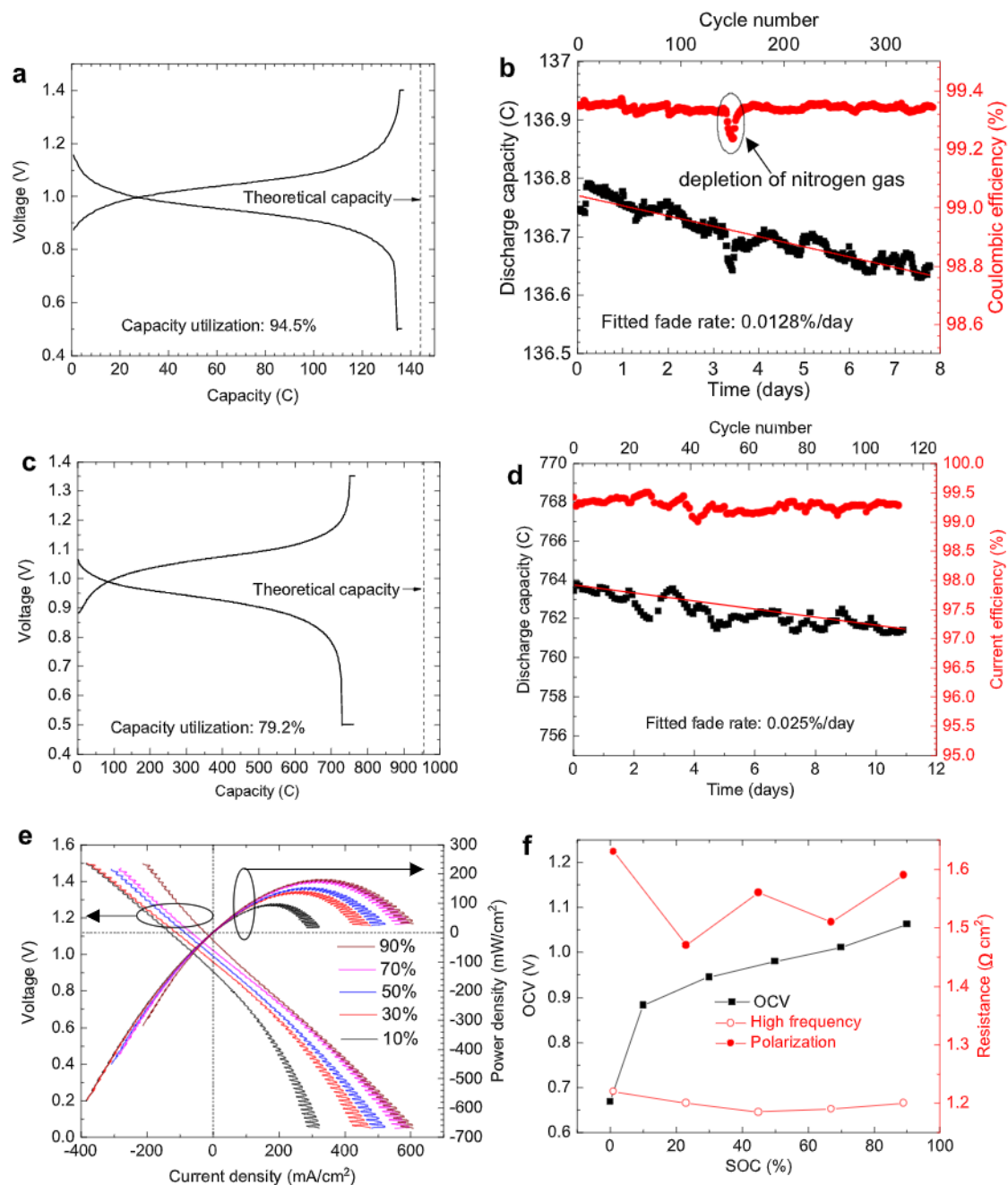


Figure 5. AQDP-based full cell measurements. (a and b) Voltage profile and long-term cycling of a 0.1 M AQDP-based full cell. Cell configuration: 7.5 mL, 0.1 M AQDP, 1 M KCl, pH 12 | 100 mL, 0.1 M $\text{K}_4\text{Fe}(\text{CN})_6$, 0.02 M $\text{K}_3\text{Fe}(\text{CN})_6$, 1 M KCl, pH 12. The cell was first charged/discharged at 30 mA/cm^2 until voltages reached 1.35 or 0.5 V and then was held at these voltages until the current density dropped to 2 mA/cm^2 . (c and d) Voltage profile and long-term cycling of a 1 M AQDP-based full cell. Cell configuration: 5 mL, 1 M AQDP, pH 12 | 100 mL, 0.5 M $\text{K}_4\text{Fe}(\text{CN})_6$, 0.1 M $\text{K}_3\text{Fe}(\text{CN})_6$, pH 12. The cell was first charged/discharged at 50 mA/cm^2 until voltages reached 1.35 or 0.5 V and then was held at these voltages until the current density dropped to 2 mA/cm^2 . (e) Cell voltage and power density versus current density at room temperature at 10%, 30%, 50%, 70%, and 90% SOC. Oscillations in current density are due to the pulsations of the peristaltic pump. (f) OCV, as well as high-frequency and polarization ASR versus SOC. For all tests, Fumasep E620(K) was used as the membrane. The pH of the electrolytes was adjusted by adding KOH pellets. Cell configuration for (e and f): 5 mL, 0.5 M AQDP, pH 12 | 100 mL, 0.5 M $\text{K}_4\text{Fe}(\text{CN})_6$, 0.1 M $\text{K}_3\text{Fe}(\text{CN})_6$, pH 12. The cell cycling tests were conducted in a N_2 -filled glovebag, and the polarization and ASR tests were conducted in a N_2 -filled glovebox.

1.47 to 1.63 $\Omega \text{ cm}^2$, due to the nearly constant membrane resistance and the varying electrolyte resistance at different SOC.

We designed and synthesized a class of carbon-linked water-soluble anthraquinones, compared the redox potentials, rate constants, diffusion coefficients, and solubility of up to 12

quinones, and selectively evaluated the thermal stabilities of four AQs. The trends that we observed are as follows:

1. The electron-withdrawing ending groups (SO_3^- , PO_3^{2-} , and CO_2^-) can affect the redox potentials of AQs with two unsaturated hydrocarbons on the chains through π -conjugation, and the redox potentials of AQDVS, AQDVP, and AQDVC are 60–80 mV higher than

those of the saturated AQs, i.e., AQDES, AQDEP, and AQDP.

2. In stark contrast, the redox potential of AQDPeS is lower than its saturated analogue AQDPS in both acidic and alkaline media. The two unsaturated C=C bonds extend the π conjugation of AQDPeS, and the methylene groups next to the C=C bonds in AQDPeS weaken the negative resonance effect of SO_3^- , thus lowering its potential.
3. For the AQs with two saturated or unsaturated straight hydrocarbons, water-solubilizing ending groups increase the redox potentials of the AQs in the order $\text{PO}_3^{2-} < \text{CO}_2^- < \text{SO}_3^-$, in agreement with theoretical predictions.
4. AQs with unsaturated chains show lower solubilities than their saturated counterparts.
5. The solubility of AQs decreases when more hydrophobic hydrocarbons are incorporated into the chains.
6. AQs with saturated and unbranched chains at high pH possess desirably low redox potentials, high solubilities, and high stability.

We further detected anthrone and anthranol formation, along with possible saturation of unsaturated chains by tautomerization. The capacity fade caused by the formation of anthrone and anthranol, however, can be regenerated. We identified 9,10-anthraquinone-2,6-dipropionic acid as a negolyte candidate given its potentially low-cost mass production and its demonstrated low temporal fade rate of 0.0128–0.025% per day when paired with a potassium ferrocyanide posolyte.

■ ASSOCIATED CONTENT

Supporting Information

The Supporting Information is available free of charge at <https://pubs.acs.org/doi/10.1021/acseenergylett.1c02504>.

Synthesis descriptions, NMR characterization of carbon-linked anthraquinone molecules, solubility tests, electrochemical cell component details and test conditions, electrochemical kinetics studies, decomposition product analyses, and cost analysis (PDF)

■ AUTHOR INFORMATION

Corresponding Authors

Roy G. Gordon – Department of Chemistry and Chemical Biology and John A. Paulson School of Engineering and Applied Sciences, Harvard University, Cambridge, Massachusetts 02138, United States; orcid.org/0000-0001-5980-268X; Email: gordon@chemistry.harvard.edu

Michael J. Aziz – John A. Paulson School of Engineering and Applied Sciences, Harvard University, Cambridge, Massachusetts 02138, United States; orcid.org/0000-0001-9657-9456; Email: maziz@harvard.edu

Authors

Yan Jing – Department of Chemistry and Chemical Biology, Harvard University, Cambridge, Massachusetts 02138, United States; orcid.org/0000-0002-5669-4609

Eric M. Fell – John A. Paulson School of Engineering and Applied Sciences, Harvard University, Cambridge, Massachusetts 02138, United States; orcid.org/0000-0003-2046-1480

Min Wu – John A. Paulson School of Engineering and Applied Sciences, Harvard University, Cambridge, Massachusetts 02138, United States

Shijian Jin – John A. Paulson School of Engineering and Applied Sciences, Harvard University, Cambridge, Massachusetts 02138, United States

Yunlong Ji – Department of Chemistry and Chemical Biology, Harvard University, Cambridge, Massachusetts 02138, United States; Present Address: School of Chemistry and Materials Science, Hangzhou Institute for Advanced Study, University of Chinese Academy of Sciences, 1 Sublane Xiangshan, Hangzhou 310024, China

Daniel A. Pollack – Department of Physics, Harvard University, Cambridge, Massachusetts 02138, United States; orcid.org/0000-0003-3909-5118

Zhijiang Tang – John A. Paulson School of Engineering and Applied Sciences, Harvard University, Cambridge, Massachusetts 02138, United States

Dian Ding – Department of Chemistry and Chemical Biology, Harvard University, Cambridge, Massachusetts 02138, United States

Meisam Bahari – John A. Paulson School of Engineering and Applied Sciences, Harvard University, Cambridge, Massachusetts 02138, United States

Marc-Antoni Goulet – John A. Paulson School of Engineering and Applied Sciences, Harvard University, Cambridge, Massachusetts 02138, United States; Present Address: Department of Chemical and Materials Engineering, Concordia University, Montreal, Quebec H3G 1M8, Canada

Tatsuhiko Tsukamoto – Department of Chemistry and Chemical Biology, Harvard University, Cambridge, Massachusetts 02138, United States

Complete contact information is available at:

<https://pubs.acs.org/doi/10.1021/acseenergylett.1c02504>

Notes

The authors declare the following competing financial interest(s): Harvard University has filed a patent application on the materials described in the paper. M.B., R.G.G., and M.J.A. have ownership stakes in Quino Energy, Inc., which might profit from these materials.

■ ACKNOWLEDGMENTS

This research was supported by the U.S. National Science Foundation through grant CBET-1914543 and by U.S. DOE award DE-AC05-76RL01830 through PNNL subcontract 535264. D.A.P. acknowledges funding support from the NSF Graduate Research Fellowship Program, nos. DGE1144152 and DGE1745303. Y.J. thanks Prof. Luke Davis for useful discussions about synthetic routes.

■ REFERENCES

- (1) Schmidt, O.; Hawkes, A.; Gambhir, A.; Staffell, I. The future cost of electrical energy storage based on experience rates. *Nature Energy* **2017**, *2* (8), 17110.
- (2) Rugolo, J.; Aziz, M. J. Electricity storage for intermittent renewable sources. *Energy Environ. Sci.* **2012**, *5* (5), 7151–7160.
- (3) Rychcik, M.; Skyllas-Kazacos, M. Characteristics of a new all-vanadium redox flow battery. *J. Power Sources* **1988**, *22*, 59–67.
- (4) Roe, S.; Menictas, C.; Skyllas-Kazacos, M. A high energy density vanadium redox flow battery with 3 M vanadium electrolyte. *J. Electrochem. Soc.* **2016**, *163* (1), A5023–A5028.
- (5) Narayan, S. R.; Nirmalchandar, A.; Murali, A.; Yang, B.; Hooper-Burkhardt, L.; Krishnamoorthy, S.; Prakash, G. K. S. Next-generation

aqueous flow battery chemistries. *Curr. Opin. Electrochem.* **2019**, *18*, 72–80.

(6) Huskinson, B. T.; Marshak, M. P.; Suh, C.; Er, S.; Gerhardt, M. R.; Galvin, C. J.; Chen, X.; Aspuru-Guzik, A.; Gordon, R. G.; Aziz, M. J. A metal-free organic-inorganic aqueous flow battery. *Nature* **2014**, *505* (7482), 195–198.

(7) Lin, K.; Chen, Q.; Gerhardt, M. R.; Tong, L.; Kim, S. B.; Eisenach, L.; Valle, A. W.; Hardee, D.; Gordon, R. G.; Aziz, M. J.; Marshak, M. P. Alkaline quinone flow battery. *Science* **2015**, *349* (6255), 1529–1532.

(8) Xu, J.; Pang, S.; Wang, X.; Wang, P.; Ji, Y. Ultrastable aqueous phenazine flow batteries with high capacity operated at elevated temperatures. *Joule* **2021**, *5* (9), 2437–2449.

(9) Wu, M.; Jing, Y.; Wong, A. A.; Fell, E. M.; Jin, S.; Tang, Z.; Gordon, R. G.; Aziz, M. J. Extremely stable anthraquinone negolytes synthesized from common precursors. *Chem* **2020**, *6*, 1432–1442.

(10) Kwabi, D. G.; Lin, K.; Ji, Y.; Kerr, E. F.; Goulet, M.-A.; De Porcellinis, D.; Tabor, D. P.; Pollack, D. A.; Aspuru-Guzik, A.; Gordon, R. G.; Aziz, M. J. Alkaline quinone flow battery with long lifetime at pH 12. *Joule* **2018**, *2* (9), 1907–1908.

(11) Ji, Y.; Goulet, M.-A.; Pollack, D. A.; Kwabi, D. G.; Jin, S.; Porcellinis, D.; Kerr, E. F.; Gordon, R. G.; Aziz, M. J. A phosphonate-functionalized quinone redox flow battery at near-neutral pH with record capacity retention rate. *Adv. Energy Mater.* **2019**, *9* (12), 1900039.

(12) Park, M.; Beh, E. S.; Fell, E. M.; Jing, Y.; Kerr, E. F.; De Porcellinis, D.; Goulet, M. A.; Ryu, J.; Wong, A. A.; Gordon, R. G.; Cho, J.; Aziz, M. J. A high voltage aqueous zinc-organic hybrid flow battery. *Adv. Energy Mater.* **2019**, *9* (25), 1900694.

(13) Beh, E. S.; De Porcellinis, D.; Gracia, R. L.; Xia, K. T.; Gordon, R. G.; Aziz, M. J. A neutral pH aqueous organic-organometallic redox flow battery with extremely high capacity retention. *ACS Energy Lett.* **2017**, *2* (3), 639–644.

(14) Jin, S.; Jing, Y.; Kwabi, D. G.; Ji, Y.; Tong, L.; De Porcellinis, D.; Goulet, M.-A.; Pollack, D. A.; Gordon, R. G.; Aziz, M. J. A water-miscible quinone flow battery with high volumetric capacity and energy density. *ACS Energy Lett.* **2019**, *4* (6), 1342–1348.

(15) Gerken, J. B.; Anson, C. W.; Preger, Y.; Symons, P. G.; Genders, J. D.; Qiu, Y.; Li, W.; Root, T. W.; Stahl, S. S. Comparison of quinone-based catholytes for aqueous redox flow batteries and demonstration of long-term stability with tetrasubstituted quinones. *Adv. Energy Mater.* **2020**, *10*, 2000340.

(16) Tong, L.; Goulet, M.-A.; Tabor, D. P.; Kerr, E. F.; De Porcellinis, D.; Fell, E. M.; Aspuru-Guzik, A.; Gordon, R. G.; Aziz, M. J. Molecular engineering of an alkaline naphthoquinone flow battery. *ACS Energy Lett.* **2019**, *4* (8), 1880–1887.

(17) Wang, C.; Li, X.; Yu, B.; Wang, Y.; Yang, Z.; Wang, H.; Lin, H.; Ma, J.; Li, G.; Jin, Z. Molecular design of fused-ring phenazine derivatives for long-cycling alkaline redox flow batteries. *ACS Energy Lett.* **2020**, *5* (2), 411–417.

(18) Murali, A.; Nirmalchandar, A.; Krishnamoorthy, S.; Hoerber-Burkhardt, L.; Yang, B.; Soloveichik, G.; Prakash, G. K. S.; Narayanan, S. R. Understanding and mitigating capacity fade in aqueous organic redox flow batteries. *J. Electrochem. Soc.* **2018**, *165* (7), A1193–A1203.

(19) Kozlov, V. A.; Ivanov, S. N.; Koifman, O. I. Solvated proton as the main reagent and a catalyst in the single-stage aromatic sulfonation and protodesulfonation of sulfonic acids. *J. Phys. Org. Chem.* **2017**, *30* (12), e3715.

(20) Xu, M.; Wan, P. Efficient photodecarboxylation of aryl-substituted phenylacetic acids in aqueous solution: a general photochemical reaction. *Chem. Commun.* **2000**, *21*, 2147–2148.

(21) Samec, J. L.; Lundstedt, A.; Sawadjoon, S. Reduction of C–O bonds by catalytic transfer hydrogenolysis. US9,382,225B2, 2016.

(22) Jing, Y.; Wu, M.; Wong, A. A.; Fell, E. M.; Jin, S.; Pollack, D. A.; Kerr, E. F.; Gordon, R. G.; Aziz, M. J. *In situ* electrosynthesis of anthraquinone electrolytes in aqueous flow batteries. *Green Chem.* **2020**, *22* (18), 6084–6092.

(23) Tabor, D. P.; Gómez-Bombarelli, R.; Tong, L.; Gordon, R. G.; Aziz, M. J.; Aspuru-Guzik, A. Mapping the frontiers of quinone stability

in aqueous media: implications for organic aqueous redox flow batteries. *J. Mater. Chem. A* **2019**, *7* (20), 12833–12841.

(24) Hu, B.; Luo, J.; Hu, M.; Yuan, B.; Liu, T. L. A pH-neutral, metal-free aqueous organic redox flow battery employing an ammonium anthraquinone anolyte. *Angew. Chem., Int. Ed.* **2019**, *58* (46), 16629–16636.

(25) Oldham, K. B.; Myland, J. C. Modelling cyclic voltammetry without digital simulation. *Electrochim. Acta* **2011**, *56* (28), 10612–10625.

(26) Bourke, A.; Miller, M. A.; Lynch, R. P.; Gao, X.; Landon, J.; Wainright, J. S.; Savinell, R. F.; Buckley, D. N. Electrode kinetics of vanadium flow batteries: contrasting responses of V^{II}–V^{III} and V^{IV}–V^V to electrochemical pretreatment of carbon. *J. Electrochem. Soc.* **2016**, *163* (1), A5097–A5105.

(27) Tenny, K. M.; Former-Cuenca, A.; Chiang, Y.-M.; Brushett, F. R. Comparing physical and electrochemical properties of different weave patterns for carbon cloth electrodes in redox flow batteries. *J. Electrochem. Energy Convers. Storage* **2020**, *17* (4), 041010.

(28) Yang, S.; Chen, Q. Quantifying electron transfer kinetics on porous carbon electrodes for redox flow batteries. *J. Electrochem. Soc.* **2020**, *167* (16), 160501.

(29) Sedenho, G. C.; De Porcellinis, D.; Jing, Y.; Kerr, E.; Mejia-Mendoza, L. M.; Vazquez-Mayagoitia, A.; Aspuru-Guzik, A.; Gordon, R. G.; Crespilho, F. N.; Aziz, M. J. Effect of molecular structure of quinones and carbon electrode surfaces on the interfacial electron transfer process. *ACS Appl. Energy Mater.* **2020**, *3* (2), 1933–1943.

(30) Yang, S.; Li, Y.; Chen, Q. Resolving electron transfer kinetics in porous electrodes via diffusion-less cyclic voltammetry. *J. Mater. Chem. A* **2021**, *9*, 14025–14031.

(31) Marcus, R. A. Electron transfer reactions in chemistry: theory and experiment. *Angew. Chem., Int. Ed. Engl.* **1993**, *32*, 1111–1121.

(32) Brushett, F. R.; Aziz, M. J.; Rodby, K. E. On lifetime and cost of redox-active organics for aqueous flow batteries. *ACS Energy Lett.* **2020**, *5*, 879–884.

(33) Kwabi, D. G.; Ji, Y.; Aziz, M. J. Electrolyte lifetime in aqueous organic redox flow batteries: A critical review. *Chem. Rev.* **2020**, *120* (14), 6467–6489.

(34) Goulet, M.-A.; Aziz, M. J. Flow battery molecular reactant stability determined by symmetric cell cycling methods. *J. Electrochem. Soc.* **2018**, *165* (7), A1466–A1477.

(35) Goulet, M.-A.; Tong, L.; Pollack, D. A.; Tabor, D. P.; Odom, S. A.; Aspuru-Guzik, A.; Kwan, E. E.; Gordon, R. G.; Aziz, M. J. Extending the lifetime of organic flow batteries via redox state management. *J. Am. Chem. Soc.* **2019**, *141* (20), 8014–8019.

(36) Jing, Y.; Zhao, E. W.; Goulet, M.-A.; Bahari, M.; Fell, E. M.; Jin, S.; Davoodi, A.; Jónsson, E.; Wu, M.; Grey, C. P.; Gordon, R. G.; Aziz, M. J. Electrochemical regeneration of anthraquinones for lifetime extension in flow batteries. *ChemRxiv*, 2021, 10.33774/chemrxiv-2021-x05x1 (accessed 2021-08-10).

(37) Pang, S.; Wang, X.; Wang, P.; Ji, Y. Biomimetic amino acid functionalized phenazine flow batteries with long lifetime at near-neutral pH. *Angew. Chem., Int. Ed.* **2021**, *60*, 5289–5298.

(38) Jin, S.; Fell, E. M.; Vina-Lopez, L.; Jing, Y.; Michalak, P. W.; Gordon, R. G.; Aziz, M. J. Near neutral pH redox flow battery with low permeability and long-lifetime phosphonated viologen active species. *Adv. Energy Mater.* **2020**, *10* (20), 2000100.

